Multiscale Imaging and Computational Modeling of Blood Flow in the Tumor Vasculature

Eugene Kim[1,2], **Spyros Stamatelos**[1], **Jana Cebulla**[3], **Zaver M. Bhujwalla**[2], **Aleksander S. Popel**[1], and **Arvind P. Pathak**[2]

[1]Department of Biomedical Engineering, The Johns Hopkins University School of Medicine, Baltimore, MD, USA

[2]JHU In vivo Cellular and Molecular Imaging Center (ICMIC), Russell H. Morgan Department of Radiology and Radiological Science, The Johns Hopkins University School of Medicine, 720 Rutland Ave, 217 Traylor Bldg., Baltimore, MD 21205, USA

[3]Department of Circulation and Medical Imaging, Norwegian University of Science and Technology, Trondheim, Norway

Abstract

The evolution in our understanding of tumor angiogenesis has been the result of pioneering imaging and computational modeling studies spanning the endothelial cell, microvasculature and tissue levels. Many of these primary data on the tumor vasculature are in the form of images from pre-clinical tumor models that provide a wealth of qualitative and quantitative information in many dimensions and across different spatial scales. However, until recently, the visualization of changes in the tumor vasculature across spatial scales remained a challenge due to a lack of techniques for integrating micro- and macroscopic imaging data. Furthermore, the paucity of three-dimensional (3-D) tumor vascular data in conjunction with the challenges in obtaining such data from patients presents a serious hurdle for the development and validation of predictive, multiscale computational models of tumor angiogenesis. In this review, we discuss the development of multiscale models of tumor angiogenesis, new imaging techniques capable of reproducing the 3-D tumor vascular architecture with high fidelity, and the emergence of "image-based models"of tumor blood flow and molecular transport. Collectively, these developments are helping us gain a fundamental understanding of the cellular and molecular regulation of tumor angiogenesis that will benefit the development of new cancer therapies. Eventually, we expect this exciting integration of multiscale imaging and mathematical modeling to have widespread application beyond the tumor vasculature to other diseases involving a pathological vasculature, such as stroke and spinal cord injury.

Keywords

Address correspondence to Arvind P. Pathak, JHU In vivo Cellular and Molecular Imaging Center (ICMIC), Russell H. Morgan Department of Radiology and Radiological Science, The Johns Hopkins University School of Medicine, 720 Rutland Ave, 217 Traylor Bldg., Baltimore, MD 21205, USA. pathak@mri.jhu.edu.

INTRODUCTION

Angiogenesis or the process of *de novo* blood vessel formation in cancer is a critical determinant of its pathophysiological characteristics, such as invasiveness, metastatic potential, and efficacy of therapies.[6,39, 109] Seminal work by Dr. Folkman has demonstrated that the progression of most solid tumors beyond 1–2 mm^3 in size is angiogenesis-dependent because of their requirement for oxygen and nutrients.[38] This switch of tumors to an angiogenic phenotype involves the upregulation of pro-angiogenic factors overwhelming the anti-angiogenic defenses of the cells.[10] Therefore, tumor progression relies upon the continual interactions between the tumor microenvironment and the host's immune system.[45]

Tumor angiogenesis is characterized by uniquely adapted endothelial cells,[17] aberrant microvasculature, [108] anomalous blood flow,[55] and disruption of homeostatic signaling pathways.[35] The evolution in our understanding of tumor angiogenesis has been the result of pioneering studies spanning the endothelial cell,[122] microvasculature[3] and tissue levels.[124] In recent years, our understanding of the angiogenic microenvironment has been revolutionized by an explosion in imaging technologies.[82] Many of these primary data on angiogenesis are in the form of images from preclinical models that provide a wealth of qualitative and quantitative information in many dimensions, and across different spatial scales.[82] Furthermore, high-throughput analyses of various cancer types have created an abundance of "-omics"data, e.g., genomics, proteomics, metabolomics. These developments have created a need for new image processing and visualization tools for extracting, comparing and integrating these data[124] (Fig. 1). The development of new imaging methods in conjunction with ever increasing and affordable computing power has ushered in a new area of bioinformatics that has been dubbed "bioimage informatics".[94]

Another factor driving multiscale imaging and modeling initiatives has been the advent of "systems biology"approaches to study disease models and pathways. For instance, the study of how genotypic interactions give rise to the function and phenotype of a biological system is inherently a multiscale problem. Therefore, there is a determined effort to develop image-based phenotyping methods,[84] particularly in murine models as they have become the workhorse of human disease models.[48] See the review by Kherlopian *et al.* [65] for a summary of imaging techniques and their utility in systems biology applications.

Furthermore, computational models have greatly refined our understanding of the microenvironmental changes that accompany tumor angiogenesis.[103] These include changes in tumor blood flow,[30,83] oxygen transport[61,111] vascular endothelial growth factor (VEGF) distribution[76] and extracellular pH.[78] However, high-resolution, high-fidelity, 3-D imaging data that simultaneously quantify tissue morphology and the molecular players involved have not been readily available. Simultaneously visualizing changes in the complex angiogenic microenvironment at different spatial scales remains a challenge due to the lack of integration between micro- and macroscopic imaging data, and the difficulty in obtaining such data from patients. Acquiring such data has been a major hurdle that needed to be overcome to further advance quantitative oncology.

This review commences with a description of imaging techniques for visualizing the 3-D tumor vasculature, followed by novel imaging strategies for characterizing the vascular phenotype at different spatial scales. Next, we recapitulate insights about the tumor vasculature that have been gleaned from pioneering mathematical models. Since the description of microcirculatory phenomena requires an understanding of their interactions with processes that occur at larger and smaller spatial scales, these traditional blood flow models have now been expanded to "multiscale"models that range from endothelial

receptors to microvascular sprouting, to the whole tissue level.[103] Therefore, we introduce 'image-based' multiscale modeling, wherein the morphological data on the organ or tumor vasculature is derived from one of several high-resolution, 3-D imaging methods. Finally, we conclude with a summary of the challenges facing this burgeoning area of research. Collectively, we expect that the integration of multi-resolution imaging and computational modeling will yield novel insights into a range of diseases involving the pathological vasculature.

IMAGING METHODS FOR VISUALIZING THE 3-D TUMOR VASCULATURE

Since pioneering neuroanatomist Ramon Cajal's early drawings of angiogenesis,[79] we have come a long way toward "capturing"the heterogeneity of the tumor vasculature. While there exists a range of methods for imaging the tumor vasculature (see the comprehensive reviews by McDonald[82] and Pathak[90]), the ensuing section highlights imaging methods capable of digitally acquiring and quantifying the 3-D architecture of these unique vessels with high fidelity.

Intravital Microscopy

Laser scanning confocal microscopy (LSCM) is a commonly used, high-resolution fluorescence imaging method. It differs from conventional fluorescence microscopy in that a focused, scanning laser source is used to excite the sample point by point, and a pinhole aperture in front of the detector and confocal (having the same focal point) to the source pinhole aperture is used to block light not emitted from the focal point. This spatial filtering of out-of-focus background fluorescence permits optical sectioning of tissue specimens up to ~100 μm thick. By scanning across a series of focal planes, a 3-D image can be constructed. LSCM has been used for intravital imaging of the vasculature in window chamber tumor xenografts labeled with fluorescent RGD-nanoparticles[87] or after intravenous injection of dextran-conjugated fluorophores.[33]

Two-photon microscopy (TPM) is another high-resolution fluorescence imaging method capable of imaging the 3-D vascular architecture *in vivo*. Two-photon fluorescence is a nonlinear optical process in which fluorescence is caused by the simultaneous absorption of two photons, each with half the requisite excitation energy. Since the probability of two photon absorption depends on the square of the light intensity, a focused ultra-short pulse laser is used to selectively excite a small region around the focal point. This provides inherent 3-D optical sectioning and reduces photobleaching and phototoxicity.[29] In addition, TPM uses near-infrared (NIR) excitation, which allows for a tissue imaging depth approaching 1 mm. TPM has been used for intravital imaging of the vasculature in window chamber tumor xenografts following intravenous injection of dextran-conjugated fluorophores to provide contrast.[1]

Optical coherence tomography (OCT) is another technique used for 3-D intravital imaging of tumor vasculature with a wider field of view (FOV) and greater depth of penetration than TPM, which come at the expense of spatial resolution. And since contrast between vessels and background tissue arises from the Doppler shift caused by the motion of circulating red blood cells, OCT does not require exogenous contrast agents. In conventional time domain OCT, a low coherence broadband light source is split into a reference arm and a sample arm; the reflected light beams from the two arms are combined and produce interference if their path lengths differ by less than the coherence length of the light source. Thus, the location within the sample from which the sample light beam is reflected can be determined by scanning the length of the reference arm and measuring the interference of the two beams, allowing a 3-D image to be reconstructed.[51] A frequency-domain OCT method called optical frequency domain imaging (OFDI) allows for more rapid imaging by employing a

frequency scanning light source while keeping the reference and sample arm lengths fixed. Depth resolution is then obtained by Fourier analysis.[127] Vakoc *et al.*[119] used TPM and OFDI to characterize the morphology of tumor vessels in various window chamber models. A comparison of the two modalities showed that TPM was capable of resolving the smallest superficial capillaries while OFDI was able to image vessels at depths of up to ~1–2 mm. For vessels larger than 12 μm in diameter as measured by TPM, the vessel diameters derived from the two modalities correlated well, but the lower spatial resolution of OFDI (~7 μm) likely resulted in partial volume effects and thus overestimation of the diameters of smaller vessels. Extensive details on intravital microscopy of the tumor vasculature can be found in reviews by Tozer *et al.*[117] and Fukumura *et al.*[40]

Magnetic Resonance Angiography

While TFM and OFDI allow high-resolution *in vivo* imaging of tumor vasculature, their limited tissue penetration restricts their use to superficial vessels or transparent window chamber models. Magnetic resonance angiography (MRA) is a method for imaging the vasculature *in vivo* without the depth limitations of optical techniques. Although MRA cannot resolve vessels at the capillary level, its spatial resolution can be increased for small animal imaging. Doblas *et al.*[31] used MRA ($102 \times 66 \times 86 \ \mu m^3$) to assess the changes in blood volume, vessel diameter and length with tumor progression in various rodent tumor models, while Figueiredo *et al.*[36] conducted time-of-flight MRA (TOF-MRA) of mouse cerebrovasculature at a spatial resolution of $31 \times 31 \times 93 \ \mu m^3$.

TOF-MRA produces images in which the vasculature appears bright without necessitating the use of exogenous contrast agents. Instead, pre-saturation radio-frequency pulses are used to attenuate the signal from stationary tissue, while unsaturated spins carried into the imaging FOV by inflowing blood exhibit higher signal, resulting in bright blood vessels. However, since this method is sensitive to flowing blood, veins and vessels in regions of low or intermittent flow such as those found in tumors can be difficult to image. Contrast enhanced (CE)-MRA is an alternative technique, which involves intravenous administration of contrast agents such as various gadolinium chelates to provide contrast between blood vessels and background tissue. The development of long-circulating blood pool contrast agents has enabled longer scan times, and thus, higher resolution and higher signal-to-noise ratio (SNR) imaging.[7] In addition, CE-MRA can achieve the same spatial resolution and higher contrast- to-noise ratio (CNR) with a shorter imaging time than TOF-MRA.[50] Van Vliet *et al.*[120] recently demonstrated the utility of high-resolution MRA by directly correlating it with digital photography and intravital microscopy in a window chamber tumor model. They found tumor angiogenesis could be mapped micro- and macroscopically *in vivo* and showed excellent correlation with the other imaging techniques. In addition, they showcased the clinical utility of CE-MRA for imaging tumor induced changes in vascularity. Finally, it should be pointed out that with MRA, one can extract and quantify changes in the 3-D morphology of blood vessels. For example, in an elegant demonstration of the clinical utility of using MRA to monitor changes in blood vessel morphology, Bullitt *et al.*[16] were able to demonstrate that 3-D vessel tortuosity measurements on vascular trees derived from MRA could predict brain metastases treatment response sooner than traditional methods.

High-resolution Ex Vivo Techniques

There are several *ex vivo* methods of imaging tumor vasculature in 3-D. Most of these methods entail the creation of a vascular "cast". A typical vascular casting procedure is described in Verli *et al.*[121]; in brief, the animal is anesthetized and then perfused, first with a solution such as heparinized saline for exsanguination, followed with a fixative such as formaldehyde, and finally with a polymerizing resin. After the cast has polymerized, a

corrosion step can be performed to macerate the surrounding tissue. The corrosion cast can then be imaged by different methods such as scanning electron microscopy (SEM) and microcomputed tomography (μCT). SEM uses a high-energy electron beam to produce very high resolution images on the scale of 1 nm. Deane and Lantos used SEM to conduct some of the earliest studies quantifying the morphological abnormalities of the endothelium of experimental brain tumors.[27] While it is not an inherently 3-D technique, stereo pairs of SEM images can be used to obtain 3-D information.[77] This SEM stereoimaging method has been used for morphometric analysis (e.g., computation of the inter-vessel distance, inter-branch distance, branching angle and vessel diameter) of vascular corrosion casts from various tumor models.[37] However, for SEM stereoimaging, 3-D reconstruction is limited to vessels that are within the "line of sight"of the electron beam.

Micro-CT (μCT), on the other hand, is a true 3-D method in which a 3-D image is reconstructed from 2-D X-ray projections taken at incremental angles around an axis of rotation. Vascular casting resins are radiopaque (i.e., strongly attenuate X-rays) and thus enable μCT imaging of the vasculature. Micro-CT is capable of imaging the vasculature of entire tumors at resolutions up to ~3 μm.[37] This is a sufficiently high resolution to image the vascular architecture down to the capillary level, as demonstrated by a study that showed excellent agreement between μCT- and SEM-measured cortical vessel diameters.[47] Another advantage of μCT is that tissue maceration is not required. While the vascular casting technique is the same, the corrosion step is excluded, which allows samples to be preserved for further study (e.g., histology). Micro-CT has also been successfully combined with MRI to create a high-resolution, 3-D atlas of the neurovasculature in a CBA mouse.[32] This rich multi-modality dataset shows the placement of the major arteries, their branches and the brain structures they feed. As one of the first 3-D atlases of the cerebral vasculature in mice, it is proving an invaluable resource for comparative studies involving the murine neurovasculature in healthy and disease models.

Risser *et al.*[107] employed a synchrotron X-ray source to conduct synchrotron radiation μCT (SRμCT) on 2.5 mm diameter cylindrical samples from 9L tumor-bearing rat brains and obtained high contrast between the vasculature and background tissue at 1.4 μm resolution. The sub-capillary spatial resolution of their 3-D images enabled them to ascertain that both tumor and normal brain vasculature display fractal organization on small spatial scales. Recently Chien *et al.*[24] employed SRμCT to profile "microangiogenesis"in a panel of subcutaneous tumor models as well as in an orthotopic pancreatic tumor model. They could assess small differences between the vasculature of pancreatic tumors derived from control or radiation activated PANC1 tumor cells. However, SRμCT is not widely available because of the need for a synchrotron for generating the high-energy X-rays necessary for imaging. Further applications of vascular imaging with μCT can be found in the review by Zagorchev *et al.*[128]

Although *ex vivo* MR microscopy or micro-MRI (μMRI) has been employed to image the vasculature of the mouse embryo[11] and adult rat brain,[62] it had not been employed to characterize the aberrant vasculature of solid tumors. Therefore, recently we developed a μMRI method to quantify the 3-D architecture of tumor blood vessels in a brain tumor model.[66] In our application, the vascular casting resin acts as a negative MRI contrast agent because it lacks the mobile water protons necessary for producing an MR signal. Thus, a 3-D image can be acquired in which blood vessels appear dark against bright background tissue. While the spatial resolution of μMRI is less than that of μCT, at 60 μm isotropic resolution we were able to quantify and distinguish the vascular phenotype of 9L brain tumor xenografts from contralateral brain as well as between brain tumors at different stages. An advantage of μMRI is that it permits the assessment of tumor vascular morphology while providing complementary, co-registered information about the tumor

microenvironment. This is achieved by exploiting different physiological MR contrast mechanisms. For example, we recently used vascular μMRI in conjunction with diffusion tensor imaging (DTI) to visualize the interplay between tumor angiogenesis and white matter reorganization that often accompanies brain tumor invasion.[91] Since μMRI is a "mesoscopic" scale imaging technique, it facilitates co-registration and bridges the spatial resolution gap between microscopic μCT and macroscopic *in vivo* MRI angiogenesis data.[22]

MULTISCALE IMAGING OF THE TUMOR VASCULATURE

As described above, the vasculature in pre-clinical tumor models has been traditionally characterized at the "cellular" scale using optical imaging methods, and the "systemic" scale using *in vivo* CT and MRI. While optical imaging and histology are powerful for quantifying changes in the tumor vasculature at submicron resolutions, they suffer from limited spatial coverage which makes co-registration with *in vivo* imaging data challenging. Also, 3-D blood vessel and tissue architecture once destroyed by sectioning is extremely difficult to reconstruct.[43] Conversely, imaging modalities such as *in vivo* MRI provide quantitative data, but lack the spatial resolution and specificity to relate changes in angiogenic parameters (e.g., tumor blood volume) to the distribution of angiogenic proteins (e.g., vascular endothelial growth factor or VEGF). Furthermore, integrating 3-D imaging data from disparate sources into computational models of tumor angiogenesis remains challenging. For example, if one wished to simulate the changes in tumor blood flow that accompany tumor progression, one would require high-resolution 3-D data describing the vascular geometry of the tumor at different time points. The scarcity of such high-quality datasets remains a serious hurdle for: (i) simultaneously visualizing changes in the angiogenic microenvironment at different spatial scales; (ii) incorporating these data in multiscale computational models of angiogenesis and their validation; (iii) phenotyping the dynamic tumor microenvironment; and (iv) obtaining an integrated, global perspective of the angiogenic microenvironment.

Some of the most exciting developments in "multiscale" imaging of the vasculature have been a consequence of advances in μCT[47] and μMRI[91] imaging techniques. Both methods permit high-resolution, 3-D, *ex vivo* imaging of the vascular network of entire organs as opposed to imaging the vasculature of excised tissue samples from limited regions of interest. Additionally, the integration of μCT and μMRI imaging with imaging modalities capable of covering complementary spatial scales permits "wide area mapping" of the vasculature.

For example, in an elegant study, Heinzer *et al.*[47] demonstrated the feasibility of true "hierarchical" imaging of the vascular network in the murine brain. In this study, the authors were able to acquire co-registered images of the murine neurovasculature over a range of spatial scales by exploiting the complementary strengths of μCT, SRμCT and SEM. To facilitate the integration of 3-D imaging data from different spatial scales, the authors utilized a specialized sample holder that facilitated registration of images from different modalities into a common image coordinate system. Large vessels visible in each image and the relative positions of regions of interests (ROIs) with respect to pins in the sample holder facilitated accurate intermodality image registration. Using this unique imaging platform, they were able to image the murine neurovasculature at spatial resolutions spanning several orders of magnitude that ranged from the endothelial cell level using SEM (~0.1 μm), through the capillary/arteriole/venule level using SRμCT (~μm) and finally to the whole brain vasculature using μCT (~10 μm) (Fig. 2). Finally, using hierarchical imaging, the authors successfully visualized and quantified differences in the morphology of the neurovasculature in a control mouse and an APP23 transgenic mouse model of Alzheimer's disease.

From the standpoint of multiscale modeling, it is desirable to integrate *in vivo* imaging data with *ex vivo* and histologic data. As illustrated in Fig. 3, this would enable: (i) bridging the spatial resolution gap between the micro- and macroscopic imaging scales; (ii) mapping the distribution of cellular factors (e.g., distribution of VEGF) obtained using optical microscopy to parametric *in vivo* MRI maps (e.g., tumor blood volume); (iii) implementation and validation of multiscale models of tumor angiogenesis (see following section for details). To facilitate the integration of ex vivo microscopic vascular data obtained using μCT (~10 μm resolution) and macroscopic blood volume data obtained in vivo with MRI, we developed a "mesoscopic"scale vascular imaging method that employs μMRI.[91] As described above, μMRI offers high 3-D imaging resolutions (~25 μm), is nondestructive, provides excellent soft tissue contrast, and preserves tissue and blood vessel architecture.[63] This platform also enabled multiscale imaging of brain tumor angiogenesis, wherein we directly compared *in vivo* MRI blood volume measurements with *ex vivo* vasculature data obtained from μMRI (Fig. 4).

Furthermore, we recently conducted multiscale angiogenesis imaging of tumor xenografts derived from the MDA-MB-231 human breast carcinoma cell line at three complementary spatial scales: (i) at the macroscopic scale with susceptibility contrast enhanced *in vivo* MRI; (ii) at the mesoscopic scale with *ex vivo* μMRI; and (iii) at the microscopic scale with μCT (Fig. 5). *In vivo* susceptibility-contrast enhanced MRI exploits the difference in intra- and extravascular magnetic susceptibility (i.e., "magnetizability"of a material placed in an external magnetic field) created by paramagnetic or superparamagnetic blood pool contrast agents such as gadolinium chelates and iron oxide nanoparticles, respectively. This susceptibility difference hastens the exponential decay of the MR signal, characterized by the transverse relaxation rate constant, which is sensitive to the underlying vasculature of the tissue being imaged.[89] It has been shown that the change in the spin echo (SE) MRI relaxation rate ΔR_2 is maximally sensitive to the *microvascular* blood volume (i.e., venules, capillaries, arterioles), while the change in the gradient echo (GE) MRIrelaxation rate ΔR_{2*} ismore sensitive to the *global* blood volume (i.e., larger vessels).[13] One can therefore create micro- and macrovascular blood volume maps to track tumor angiogenesis *in vivo*. We then employed μMRI as an "integrator"(as described in Fig. 3) to bridge the resolution gap between μCT and *in vivo* MRI blood volume data.[22] To achieve this, we first extracted the 3-D tumor vasculature from μMRI and μCT data as described in Kim *et al*.[66] and Cebulla *et al*.[22] Next, 3-D μMRI data were co-registered to the *in vivo* MRI data using images from the first echo time (TE). We then co-registered the μCT vascular data to the μMRI vascular data using landmarks placed on large vessels. Fractional blood volume (FBV) maps were computed from high-resolution μMRI and μCT vascular data by re-sampling these data onto the *in vivo* MRI spatial grid, and calculating the fractional occupancy of vessels in each *in vivo* voxel as described in Kim *et al*.[66] and Cebulla *et al*.[22] The FBV calculated from μMRI systematically overestimated the values calculated from μCT (Figs. 5b–5c). This was likely the result of partial volume effects resulting from the coarser spatial resolution of μMRI relative to μCT. And while two disparate contrast mechanisms were used to generate the *in vivo* and *ex vivo* FBV maps, there was good qualitative correspondence between the three modalities (Figs. 5a–5c). Additionally, tumor rim and core ROIs were identified using morphological erosion of the tumor 'mask' such that the numbers of pixels in the two regions were approximately equal. It was found that consistent with the vascular phenotype of this human breast cancer model, the FBV in the tumor core was significantly lower compared to the rim at all three spatial scales (Figs. 5d–5f).

In recent years there has been a concerted effort toward acquiring multiscale data in a range of preclinical disease models. A major driving force in this integration has been the development of novel optical [34] and molecular imaging techniques.[92] Innovations include the development of brighter, more photostable, and switchable contrast agents that enable

imaging of gene expression, protein compartmentalization, target localization, and receptor kinetics. Collectively, these advances have facilitated the integration of traditional imaging techniques with "-omic" approaches for elucidating the systems biology of cells, entire organ systems and animals. As this review is focused on multiscale, 3-D imaging of the tumor vasculature, readers are referred to outstanding reviews by Megason *et al.*[84] and Du *et al.*[34] for detailed treatment of these topics.

INSIGHTS ABOUT THE TUMOR VASCULATURE FROM MATHEMATICAL MODELING

The acquisition and reconstruction of "wide-area", 3-D microvascular networks from high-resolution imaging data is technically challenging and computationally intensive and such data are only now becoming available. Thus, in the past researchers had to employ *in silico* synthesized vascular networks to study hemodynamics in the microcirculation.[8,15,54,115] Modeling of microvascular hemodynamics has been reviewed in Lee and Smith[68] and Popel and Johnson.[96] Blood flowing in microvessels exhibits non-Newtonian rheological properties, e.g., the effective viscosity is dependent on vessel diameter. Based on experimental measurements of blood flow in rat mesentery, Pries, Secomb and co-authors have derived empirical relationships to account for the *in vivo* Fahraeus effect (tube hematocrit lower than discharge hematocrit), Fahraeus-Lindqvist effect (effective viscosity in a microvessel lower than bulk viscosity) and phase separation effects of red blood cells in bifurcations.[101,102] Subsequently, their models have included the remodeling of blood vessels due to hemodynamic and metabolic stimuli, as well as the effect of the endothelial surface layer (ESL) on effective viscosity.[99,100] The Pries and Secomb analysis has been applied to calculations of microvascular blood flow and hematocrit distribution in skeletal muscle,[9,71,118] brain,[74,75] heart,[69] lung,[126] eye[42] and other tissues and organs; constant Newtonian viscosity calculations assuming Poiseuille flow in vascular segments have been carried out in the heart, taking into account myocardial contractions.[26]

In contrast to the vasculature of healthy tissues, a hallmark of the tumor microvasculature is its highly irregular morphology.[67] Consequently, the distribution of blood,[55] oxygen and nutrients is extremely heterogeneous, leading to the creation of hypoxic regions in the tumor.[40,98] Hyperpermeable tumor vessels result in elevated interstitial fluid pressure that negatively affects drug delivery, targeted chemotherapy and radiation therapy.[41] Therefore, mathematical simulations of microvascular hemodynamics at the whole-tumor level will benefit the development and optimization of new therapies for inhibiting cancer growth and angiogenesis.

Jain has proposed that anti-angiogenic therapy can normalize tumor blood flow by reducing vascular heterogeneity and allowing more efficient delivery of anticancer agents.[56] On the other hand, excessive anti-angiogenic therapy could ultimately lead to destruction of tumor blood vessels and enhance the tumor's resistance to therapy. Therefore, it would be invaluable to be able to identify the "window of opportunity" for vascular normalization.[20,56,57] Based on these concepts, Jain and coworkers developed a mathematical model and showed that anti-angiogenic therapy can affect a number of key aspects of the tumor microenvironment, such as interstitial fluid pressure and vascular permeability.[60] Wu *et al.*[125] developed a 3-D computational framework to predict the effects of vascular normalization on a synthetic tumor vascular network induced by anti-angiogenic therapy. In conjunction with physiologically derived parameters, a detailed knowledge of the 3-D geometrical features of the tumor vessel network would enable more realistic simulations of blood flow in every segment of the *de facto* tumor vascular network.[59] Furthermore, computational models of blood flow, shear rate and hematocrit have the potential to quantify the functional and structural heterogeneity and remodeling of tumor

vascular networks in comparison to normal ones.[97,110] Due to the disorganized nature of tumor vasculature, microvessel density alone is not an adequate biomarker of successful anti-angiogenic therapy. [58] As a result, a number of functional and morphological indices have been proposed to assess the efficacy of drug delivery[5,97] and anti-angiogenic therapy[90] in tumors. Finally, predictions of shear stress values across the tumor vasculature can provide valuable information related to the mechanotransduced activation of genes related to angiogenesis.[64]

Collectively, these computational advances have the potential to: (i) contribute to a "systems-level"view of angiogenesis; (ii) increase the efficacy with which circulating pharmaceutical agents can be administered[12]; and (iii) aide in the development of clinical blood biomarkers (e.g., cancer proteins secreted into the blood) of cancer detection.[49]

IMAGE-BASED MODELS OF TISSUEAND ORGAN-LEVEL BLOOD FLOW

The advances in imaging described above, together with multiscale models of blood flow constitute a new computational framework for elucidating the function of various organ systems under normal and pathophysiological conditions.[52] An accurate quantitative description of the 3-D blood vessel architecture is necessary for numerically solving partial differential equations of fluid dynamics. Advances in processing power and high-resolution imaging have resulted in sophisticated new image-based "macroscale"(i.e., at the spatial scale of arteries and assuming Newtonian properties of blood) computational models of blood flow in vascular networks to elucidate systemic disease states (Fig. 6). These approaches span from one-dimensional (1-D) models up to 3-D models attempting to characterize the entire arterial network by applying the appropriate boundary conditions (Table 1). For example, Zhou *et al.*[129] applied a 3-D finite element method (FEM) to predict cardiovascular flow in a whole-body model based on vascular data derived from CT imaging. Similarly, elegant multidomain approaches have been developed to describe 3-D hemodynamics in major arteries. In these multiscale systems, the computational fluid dynamic (CFD) models are linked to lumped parameter (e.g., windkessel) models to account for the impedance of various organs and the downstream vascular bed.[123]

Theoretical approaches to describe the dynamics of blood flow in image-based vasculature of several physiological subsystems have been reported. Grinberg and Karniadakis applied a 3-D spectral element method to simulate the intracranial blood flow network. In this model they imposed Resistance–Capacitance (RC) and RCR (two- and three-element windkessel models) pressure boundary conditions for the closure linking the outlet domain resistances with their flow rates ratio.[44] A 3-D FEM approach was used by Tang *et al.*[116] to describe blood flow in major pulmonary arteries based on MRI-acquired vessel structure. A summary of representative macroscale hemodynamic studies using image-derived vascular geometries is presented in Table 1.

Recently, Lorthois *et al.*[74,75] simulated blood flow and predicted hematocrit distribution in a human cerebral microvascular network, comparing different boundary conditions. The data for this study were derived from confocal microscopy of thick sections of India ink-injected human brain.[21] Benedict *et al.*[9] also used confocal microscopy to obtain vascular data on immunostained skeletal muscle and performed hemodynamic simulations. SRµCT-derived vascular data was used by Reichold *et al.*[105] to simulate cerebral blood flow. Micro-CT data were used by Lee and Smith to implement a novel approach linking blood flow and hematocrit in a coronary microvascular network model.[69] Yang *et al.*[126] also employed µCT-derived 3-D vascular data to simulate the hemodynamics of the rat placenta and lung vasculature (Table 2).

IMAGE-BASED MODELING OF TUMOR BLOOD FLOW

Several factors have contributed to the rapid progress of multiscale computational models of solid tumors, e.g., the development of new modeling methodologies, such as agent-based modeling and the integration of the molecular, cellular, and tissue scales. Agent-based models represent a class of computational models in which a discrete rule-based approach is used to simulate the interaction of individual entities of interest (e.g., cells, macromolecules etc.) with one another and with their microenvironment. The rules that dictate the behavior of these agents can be defined more succinctly due to the availability of high-throughput genomic and proteomic data. These advances in modeling tumor growth and progression are summarized in Chaplain *et al.*,[23] Hatzikirou *et al.*,[46] Anderson and Quaranta,[2] Byrne,[18] Deisboeck *et al.*,[28] Rejniak and Anderson,[106] Stefanini *et al.*[114]

While *ex vivo* and *in vivo* optical imaging data have been employed to develop multiscale 3-D models of tumor growth,[25,95] models of tumor blood flow based on high-resolution imaging data are only emerging.[86] We have recently applied the hemorheological formulation described above to the "wide-area"digitized microvasculature of a human triple-negative breast cancer xenograft model acquired with 8 μm spatial resolution using μCT.[22] The tumor was excised 5 weeks after orthotopically inoculating MDA-MB-231 human breast cancer cells in the mammary fat pad of SCID mice. Details of the experimental procedure, image acquisition and processing are described in the section on Multiscale Imaging above. Following segmentation of the tumor vasculature, we identified the topological features of the microvascular network (e.g., node position vectors and adjacency matrix) and filtered any morphological discrepancies present in the images.[21] The reconstructed network (Fig. 6a) exhibited all the known characteristics of breast tumor microvascular morphology such as trifurcations, tortuosity, self-loops and blind ends.[70] Pressure boundary conditions were imposed in hemodynamic simulations. The Amira (Visage Imaging) software package was used for visualization of the results. Figures 6b and 6e illustrate the simulated microvascular flow rate and pressure drop in each of the segments of the μCT-derived tumor vasculature. Figure 6f illustrates the distributions of vessel radius and flow rate for two ROIs selected in the tumor rim (Fig. 6c) and core (Fig. 6d), respectively. Our hemodynamic analysis revealed functional "shunting"(i.e., high flow, low resistance paths) that is often observed in tumor vascular networks. In addition, it indicated the remarkably elevated vascularization and blood flow in the rim compared to the core of the tumor vascular network. These results are consistent with the ROI analysis of FBV obtained from multiscale imaging presented in Fig. 5. Much remains to be accomplished to make comprehensive and validated predictions at different stages of tumor growth and for different tumor types, with and without therapeutic interventions.

CHALLENGES AND FUTURE STEPS

While considerable advances have been made in the fields of multiscale imaging and modeling, significant challenges still remain. It remains necessary to rigorously validate the predictions of multiscale blood flow models on a scale similar to that employed in the simulations. Such validation would involve multiscale imaging that spans from the capillary to the macro-vascular scale. For example, one could employ laser speckle imaging[104] or microsphere-based techniques[80] to assess microvascular perfusion, and *in vivo* MRI[89] or CT and ultrasound[14] to assess perfusion at the whole tumor/organ level. It will also be necessary to develop new image processing schemes and databases for seamlessly integrating and mining these multiscale datasets. We will need to develop strategies for exploiting the availability of online repositories of gene expression and proteomic data (e.g., the Allen Brain Atlas Project[88]) for integration into, and validation of these models. Finally, it will be necessary to establish a unified framework for disseminating these multiscale models and

imaging data to the widest possible audience. Taking these future steps will herald a new understanding of phenomena as diverse as the tumor microenvironment, structure–function relationships in disease and drug delivery.

CONCLUSION

Although focused on the tumor vasculature, the multiscale imaging methods described here can be employed in a variety of disease models that involve a pathological vasculature, e.g., stroke and spinal cord injury. The eventual integration of hierarchical imaging platforms with widely available genomic databases will enable systems biology researchers to gain insights into a range of issues, such as the mechanisms of resistance to anti-angiogenic therapies. When incorporated in computational models of MR susceptibility contrast such as the finite perturber method,[93] multiscale data could help elucidate the biophysical relationship between the MRI signal and the underlying vasculature. This would facilitate the development of more accurate clinical biomarkers of angiogenesis and anti-angiogenic therapy. Moreover, image-based blood flow modeling of the tumor vasculature provides valuable information on the hemodynamic properties of the network that influence endothelial sprouting and vascular remodeling.[98,112] This will also enable development of multiscale mathematical platforms of tumor growth and angiogenesis based on detailed experimental data, without the need to rely on idealized vascular structures.[19,73,95] Multiscale modeling can be exploited to assess various anti-tumor and anti-angiogenic treatment scenarios, as well as guide the administration of these agents. We believe that multiscale imaging and modeling will be an invaluable resource for researchers for years to come, and will greatly enhance our understanding of the complex system that is the tumor microenvironment.

Acknowledgments

REFERENCES

1. Ameer-Beg SM, Barber PR, Hodgkiss RJ, Locke RJ, Newman RG, Tozer GM, Vojnovic B, Wilson J. Application of multiphoton steady state and lifetime imaging to mapping of tumour vascular architecture in vivo. Proc. SPIE. 2002; 4620:85–95.

2. Anderson AR, Quaranta V. Integrative mathematical oncology. Nat. Rev. Cancer. 2008; 8(3):227–234. [PubMed: 18273038]

3. Andres AC, Djonov V. The mammary gland vasculature revisited. J. Mammary Gland Biol. Neoplasia. 2010; 15(3):319–328. [PubMed: 20706777]

4. Augsburger L, Reymond P, Rufenacht DA, Stergiopulos N. Intracranial stents being modeled as a porous medium: flow simulation in stented cerebral aneurysms. Ann. Biomed. Eng. 2011; 39(2):850–863. [PubMed: 21042856]

5. Baish JW, Stylianopoulos T, Lanning RM, Kamoun WS, Fukumura D, Munn LL, Jain RK. Scaling rules for diffusive drug delivery in tumor and normal tissues. Proc. Natl Acad. Sci. USA. 2011; 108(5):1799–1803. [PubMed: 21224417]

6. Banerjee S, Dowsett M, Ashworth A, Martin LA. Mechanisms of disease: angiogenesis and the management of breast cancer. Nat. Clin.Pract.Oncol. 2007; 4(9):536–550. [PubMed: 17728712]

7. Barrett T, Kobayashi H, Brechbiel M, Choyke PL. Macromolecular MRI contrast agents for imaging tumor angiogenesis. Eur. J. Radiol. 2006; 60(3):353–366. [PubMed: 16930905]

8. Beard DA, Bassingthwaighte JB. The fractal nature of myocardial blood flow emerges from a wholeorgan model of arterial network. J. Vasc. Res. 2000; 37(4):282–296. [PubMed: 10965227]

9. Benedict KF, Coffin GS, Barrett EJ, Skalak TC. Hemodynamic systems analysis of capillary network remodeling during the progression of type 2 diabetes. Microcirculation. 2011; 18(1):63–73. [PubMed: 21166927]

10. Bergers G, Benjamin LE. Tumorigenesis and the angiogenic switch. Nat. Rev. Cancer. 2003; 3(6): 401–410. [PubMed: 12778130]

11. Berrios-Otero CA, Wadghiri YZ, Nieman BJ, Joyner AL, Turnbull DH. Three-dimensional micro-MRI analysis of cerebral artery development in mouse embryos. Magn. Reson. Med. 2009; 62(6): 1431–1439. [PubMed: 19859945]

12. Bhise NS, Shmueli RB, Sunshine JC, Tzeng SY, Green JJ. Drug delivery strategies for therapeutic angiogenesis and antiangiogenesis. Expert. Opin. Drug. Deliv. 2011; 8(4):485–504. [PubMed: 21338327]

13. Boxerman JL, Hamberg LM, Rosen BR, Weisskoff RM. MR contrast due to intravascular magnetic susceptibility perturbations. Magn. Reson. Med. 1995; 34(4):555–566. [PubMed: 8524024]

14. Broumas AR, Pollard RE, Bloch SH, Wisner ER, Griffey S, Ferrara KW. Contrast-enhanced computed tomography and ultrasound for the evaluation of tumor blood flow. Invest. Radiol. 2005; 40(3):134–147. [PubMed: 15714088]

15. Bui A, Sutalo ID, Manasseh R, Liffman K. Dynamics of pulsatile flow in fractal models of vascular branching networks. Med. Biol. Eng. Comput. 2009; 47(7):763–772. [PubMed: 19468774]

16. Bullitt E, Lin NU, Smith JK, Zeng D, Winer EP, Carey LA, Lin W, Ewend MG. Blood vessel morphologic changes depicted with MR angiography during treatment of brain metastases: a feasibility study. Radiology. 2007; 245(3):824–830. [PubMed: 17954616]

17. Butler JM, Kobayashi H, Rafii S. Instructive role of the vascular niche in promoting tumour growth and tissue repair by angiocrine factors. Nat. Rev. Cancer. 2010; 10(2):138–146. [PubMed: 20094048]

18. Byrne HM. Dissecting cancer through mathematics: from the cell to the animal model. Nat. Rev. Cancer. 2010; 10(3):221–230. [PubMed: 20179714]

19. Cai Y, Xu S, Wu J, Long Q. Coupled modelling of tumour angiogenesis, tumour growth and blood perfusion. J. Theor. Biol. 2011; 279(1):90–101. [PubMed: 21392511]

20. Carmeliet P, Jain RK. Principles and mechanisms of vessel normalization for cancer and other angiogenic diseases. Nat. Rev. Drug. Discov. 2011; 10(6):417–427. [PubMed: 21629292]

21. Cassot F, Lauwers F, Fouard C, Prohaska S, Lauwers-Cances V. A novel three-dimensional computerassisted method for a quantitative study of microvascular networks of the human cerebral cortex. Microcirculation. 2006; 13(1):1–18. [PubMed: 16393942]

22. Cebulla J, Kim E, Zhang J, Pathak AP. Multiscale imaging of angiogenesis in a breast cancer model. Proc. Int. Soc Mag Reson Med. 2011; 19(758)

23. Chaplain, MAJ.; McDougall, SR.; Anderson, ARA. Blood flow and tumour-induced angiogenesis: dynamically adapting vascular networks. In: Jackson, TL., editor. Modeling Tumor Vasculature: Molecular, Cellular, and Tissue Level Aspects and Implications. New York: Springer; 2012. p. 167-212.

24. Chien CC, Kempson IM, Wang CL, Chen HH, Hwu Y, Chen NY, Lee TK, Petibois C, Tsai KK, Liu MS, Chang KY, Yang CS, Margaritondo G. Complete microscale profiling of tumor microangiogenesis A microradiological methodology reveals fundamental aspects of tumor angiogenesis and yields an array of quantitative parameters for its characterization. Biotechnol. Adv. 2011

25. Choe SC, Zhao G, Zhenyuan Zhao Z, Rosenblatt JD, Cho H-M, Shin S-U, Johnson NF. Model for in vivo progression of tumors based on co-evolving cell population and vasculature. Sci. Rep. 2011; 1(31):1–8. [PubMed: 22355520]

26. Cookson AN, Lee J, Michler C, Chabiniok R, Hyde E, Nordsletten DA, Sinclair M, Siebes M, Smith NP. A novel porous mechanical framework for modelling the interaction between coronary perfusion and myocardial mechanics . J. Biomech. 2011

27. Deane BR, Lantos PL. The vasculature of experimental brain tumours. Part 1. A sequential light and electron microscope study of angiogenesis. J. Neurol. Sci. 1981; 49(1):55–66. [PubMed: 7205320]

28. Deisboeck TS, Zhang L, Yoon J, Costa J. In silico cancer modeling: is it ready for prime time? Nat. Clin. Pract. Oncol. 2009; 6(1):34–42. [PubMed: 18852721]

29. Denk W, Strickler JH, Webb WW. Two-photon laser scanning fluorescence microscopy. Science. 1990; 248(4951):73–76. [PubMed: 2321027]

30. Dewhirst MW, Tso CY, Oliver R, Gustafson CS, Secomb TW, Gross JF. Morphologic and hemodynamic comparison of tumor and healing normal tissue microvasculature. Int. J. Radiat. Oncol. Biol. Phys. 1989; 17(1):91–99. [PubMed: 2745213]

31. Doblas S, He T, Saunders D, Pearson J, Hoyle J, Smith N, Lerner M, Towner RA. Glioma morphology and tumor-induced vascular alterations revealed in seven rodent glioma models by in vivo magnetic resonance imaging and angiography. J. Magn. Reson. Imaging. 2010; 32(2):267–275. [PubMed: 20677250]

32. Dorr A, Sled JG, Kabani N. Three-dimensional cerebral vasculature of the CBA mouse brain: a magnetic resonance imaging and micro computed tomography study. Neuroimage. 2007; 35(4):1409–1423. [PubMed: 17369055]

33. Dreher MR, Liu W, Michelich CR, Dewhirst MW, Yuan F, Chilkoti A. Tumor vascular permeability, accumulation, and penetration of macromolecular drug carriers. J. Natl Cancer Inst. 2006; 98(5):335–344. [PubMed: 16507830]

34. Du W, Wang Y, Luo Q, Liu BF. Optical molecular imaging for systems biology: from molecule to organism. Anal. Bioanal. Chem. 2006; 386(3):444–457. [PubMed: 16850295]

35. Ferrara N. VEGF and the quest for tumour angiogenesis factors. Nat. Rev. Cancer. 2002; 2(10):795–803. [PubMed: 12360282]

36. Figueiredo G, Brockmann C, Boll H, Heilmann M, Schambach SJ, Fiebig T, Kramer M, Groden C, Brockmann MA. Comparison of digital subtraction angiography, micro-computed tomography angiography and magnetic resonance angiography in the assessment of the cerebrovascular system in live mice. Clin. Neuroradiol. 2011

37. Folarin AA, Konerding MA, Timonen J, Nagl S, Pedley RB. Three-dimensional analysis of tumour vascular corrosion casts using stereoimaging and micro-computed tomography. Microvasc. Res. 2010; 80(1):89–98. [PubMed: 20303995]

38. Folkman J. Tumor angiogenesis: therapeutic implications. N. Engl. J. Med. 1971; 285(21):1182–1186. [PubMed: 4938153]

39. Folkman J. The influence of angiogenesis research on management of patients with breast cancer. Breast Cancer Res. Treat. 1995; 36(2):109–118. [PubMed: 8534860]

40. Fukumura D, Duda DG, Munn LL, Jain RK. Tumor microvasculature and microenvironment: novel insights through intravital imaging in pre-clinical models. Microcirculation. 2010; 17(3):206–225. [PubMed: 20374484]

41. Fukumura D, Jain RK. Tumor microvasculature and microenvironment: targets for anti-angiogenesis and normalization. Microvasc. Res. 2007; 74(2-3):72–84. [PubMed: 17560615]

42. Ganesan P, He S, Xu H. Analysis of retinal circulation using an image-based network model of retinal vasculature. Microvasc. Res. 2010; 80(1):99–109. [PubMed: 20156460]

43. Gijtenbeek JM, Wesseling P, Maass C, Burgers L, van der Laak JA. Three-dimensional reconstruction of tumor microvasculature: simultaneous visualization of multiple components in paraffin-embedded tissue. Angiogenesis. 2005; 8(4):297–305. [PubMed: 16328157]

44. Grinberg L, Cheever E, Anor T, Madsen JR, Karniadakis GE. Modeling blood flow circulation in intracranial arterial networks: a comparative 3D/1D simulation study. Ann. Biomed. Eng. 2011; 39(1):297–309. [PubMed: 20661645]

45. Hanahan D, Weinberg RA. Hallmarks of cancer: the next generation. Cell. 2011; 144(5):646–674. [PubMed: 21376230]

46. Hatzikirou H, Chauviere A, Bauer AL, Leier A, Lewis MT, Macklin P, Marquez-Lago TT, Bearer EL, Cristini V. Integrative physical oncology. Wiley Interdiscip Rev. Syst. Biol. Med. 2012; 4(1):1–14. [PubMed: 21853537]

47. Heinzer S, Krucker T, Stampanoni M, Abela R, Meyer EP, Schuler A, Schneider P, Muller R. Hierarchical microimaging for multiscale analysis of large vascular networks. Neuroimage. 2006; 32(2):626–636. [PubMed: 16697665]

48. Henkelman RM. Systems biology through mouse imaging centers: experience and new directions. Annu. Rev. Biomed. Eng. 2010; 12:143–166. [PubMed: 20415591]

49. Hori SS, Gambhir SS. Mathematical model identifies blood biomarker-based early cancer detection strategies and limitations. Sci. Trans. Med. 2011; 3(109):109ra116.

50. Howles GP, Ghaghada KB, Qi Y, Mukundan S Jr, Johnson GA. High-resolution magnetic resonance angiography in the mouse using a nanoparticle blood-pool contrast agent. Magn. Reson. Med. 2009; 62(6):1447–1456. [PubMed: 19902507]

51. Huang D, Swanson EA, Lin CP, Schuman JS, Stinson WG, Chang W, Hee MR, Flotte T, Gregory K, Puliafito CA, et al. Optical coherence tomography. Science. 1991; 254(5035):1178–1181. [PubMed: 1957169]

52. Humphrey JD, Taylor CA. Intracranial and abdominal aortic aneurysms: similarities, differences, and need for a new class of computational models. Annu. Rev. Biomed. Eng. 2008; 10:221–246. [PubMed: 18647115]

53. Huo Y, Choy JS, Svendsen M, Sinha AK, Kassab GS. Effects of vessel compliance on flow pattern in porcine epicardial right coronary arterial tree. J. Biomech. 2009; 42(5):594–602. [PubMed: 19195659]

54. Huo Y, Kaimovitz B, Lanir Y, Wischgoll T, Hoffman JI, Kassab GS. Biophysical model of the spatial heterogeneity of myocardial flow. Biophys. J. 2009; 96(10):4035–4043. [PubMed: 19450475]

55. Jain RK. Determinants of tumor blood flow: a review. Cancer Res. 1988; 48(10):2641–2658. [PubMed: 3282647]

56. Jain RK. Normalization of tumor vasculature: an emerging concept in antiangiogenic therapy. Science. 2005; 307(5706):58–62. [PubMed: 15637262]

57. Jain RK. Taming vessels to treat cancer. Sci. Am. 2008; 298(1):56–63. [PubMed: 18225696]

58. Jain RK, Duda DG, Willett CG, Sahani DV, Zhu AX, Loeffler JS, Batchelor TT, Sorensen AG. Biomarkers of response and resistance to antiangiogenic therapy. Nat. Rev. Clin. Oncol. 2009; 6(6):327–338. [PubMed: 19483739]

59. Jain RK, Stylianopoulos T. Delivering nanomedicine to solid tumors. Nat. Rev. Clin. Oncol. 2010; 7(11):653–664. [PubMed: 20838415]

60. Jain RK, Tong RT, Munn LL. Effect of vascular normalization by antiangiogenic therapy on interstitial hypertension, peritumor edema, and lymphatic metastasis: insights from a mathematical model. Cancer Res. 2007; 67(6):2729–2735. [PubMed: 17363594]

61. Ji JW, Tsoukias NM, Goldman D, Popel AS. A computational model of oxygen transport in skeletal muscle for sprouting and splitting modes of angiogenesis. J. Theor. Biol. 2006; 241(1):94–108. [PubMed: 16388825]

62. Johnson GA, Benveniste H, Engelhardt RT, Qiu H, Hedlund LW. Magnetic resonance microscopy in basic studies of brain structure and function. Ann. N. Y. Acad. Sci. 1997; 820:139–147. [PubMed: 9237453]

63. Johnson GA, Cofer GP, Gewalt SL, Hedlund LW. Morphologic phenotyping with MR microscopy: the visible mouse. Radiology. 2002; 222(3):789–793. [PubMed: 11867802]

64. Kamoun WS, Chae SS, Lacorre DA, Tyrrell JA, Mitre M, Gillissen MA, Fukumura D, Jain RK, Munn LL. Simultaneous measurement of RBC velocity, flux, hematocrit and shear rate in vascular networks. Nat. Methods. 2010; 7(8):655–660. [PubMed: 20581828]

65. Kherlopian AR, Song T, Duan Q, Neimark MA, Po MJ, Gohagan JK, Laine AF. A review of imaging techniques for systems biology. BMC Syst. Biol. 2008; 2(74)

66. Kim E, Zhang J, Hong K, Benoit NE, Pathak AP. Vascular phenotyping of brain tumors using magnetic resonance microscopy (muMRI). J. Cereb. Blood Flow Metab. 2011; 31(7):1623–1636. [PubMed: 21386855]

67. Konerding MA, Malkusch W, Klapthor B, van Ackern C, Fait E, Hill SA, Parkins C, Chaplin DJ, Presta M, Denekamp J. Evidence for characteristic vascular patterns in solid tumours: quantitative studies using corrosion casts. Br. J. Cancer. 1999; 80(5-6):724–732. [PubMed: 10360650]

68. Lee J, Smith NP. Theoretical modeling in hemodynamics of microcirculation. Microcirculation. 2008; 15(8):699–714. [PubMed: 18720227]

69. Lee J, Smith N. Development and application of a one-dimensional blood flow model for microvascular networks. Proc. Inst. Mech. Eng. H. 2008; 222(4):487–511. [PubMed: 18595360]

70. Less JR, Skalak TC, Sevick EM, Jain RK. Microvascular architecture in a mammary carcinoma: branching patterns and vessel dimensions. Cancer Res. 1991; 51(1):265–273. [PubMed: 1988088]

71. Liu G, Qutub AA, Vempati P, Mac Gabhann F, Popel AS. Module-based multiscale simulation of angiogenesis in skeletal muscle. Theor. Biol. Med. Model. 2011; 8(6)

72. Liu D, Wood NB, Witt N, Hughes AD, Thom SA, Xu XY. Computational analysis of oxygen transport in the retinal arterial network. Curr. Eye Res. 2009; 34(11):945–956. [PubMed: 19958111]

73. Lloyd BA, Szczerba D, Rudin M, Szekely G. A computational framework for modelling solid tumour growth. Philos. Trans. A Math. Phys. Eng. Sci. 2008; 366(1879):3301–3318. [PubMed: 18593664]

74. Lorthois S, Cassot F, Lauwers F. Simulation study of brain blood flow regulation by intra-cortical arterioles in an anatomically accurate large human vascular network. Part II: flow variations induced by global or localized modifications of arteriolar diameters. Neuroimage. 2011; 54(4): 2840–2853. [PubMed: 21047557]

75. Lorthois S, Cassot F, Lauwers F. Simulation study of brain blood flow regulation by intra-cortical arterioles in an anatomically accurate large human vascular network: part I: methodology and baseline flow. Neuroimage. 2011; 54(2):1031–1042. [PubMed: 20869450]

76. Mac Gabhann F, Ji JW, Popel AS. Computational model of vascular endothelial growth factor spatial distribution in muscle and pro-angiogenic cell therapy. PLoS Comput. Biol. 2006; 2(9):e127. [PubMed: 17002494]

77. Malkusch W, Konerding MA, Klapthor B, Bruch J. A simple and accurate method for 3-D measurements in microcorrosion casts illustrated with tumour vascularization. Anal. Cell. Pathol. 1995; 9(1):69–81. [PubMed: 7577757]

78. Martin NK, Gaffney EA, Gatenby RA, Gillies RJ, Robey IF, Maini PK. A mathematical model of tumour and blood pHe regulation: the HCO3 2/ CO2buffering system. Math. Biosci. 2011; 230(1): 1–11. [PubMed: 21167185]

79. Martinez A, Marin VG, Junquera SR, Martinez- Murillo R, Freire M. The contributions of Santiago Ramon y Cajal to cancer research�100 years on. Nat. Rev. Cancer. 2005; 5(11):904–909. [PubMed: 16327767]

80. Marxen M, Sled JG, Yu LX, Paget C, Henkelman RM. Comparing microsphere deposition and flow modeling in 3D vascular trees. Am. J. Physiol. Heart Circ. Physiol. 2006; 291(5):H2136–H2141. [PubMed: 16766647]

81. Marzo A, Singh P, Reymond P, Stergiopulos N, Patel U, Hose R. Influence of inlet boundary conditions on the local haemodynamics of intracranial aneurysms. Comput. Methods Biomech. Biomed. Eng. 2009; 12(4):431–444.

82. McDonald DM, Choyke PL. Imaging of angiogenesis: from microscope to clinic. Nat. Med. 2003; 9(6):713–725. [PubMed: 12778170]

83. McDougall SR, Anderson AR, Chaplain MA, Sherratt JA. Mathematical modelling of flow through vascular networks: implications for tumour-induced angiogenesis and chemotherapy strategies. Bull. Math. Biol. 2002; 64(4):673–702. [PubMed: 12216417]

84. Megason SG, Fraser SE. Imaging in systems biology. Cell. 2007; 130(5):784–795. [PubMed: 17803903]

85. Morbiducci U, Gallo D, Massai D, Consolo F, Ponzini R, Antiga L, Bignardi C, Deriu MA, Redaelli A. Outflow conditions for image-based hemodynamic models of the carotid bifurcation: implications for indicators of abnormal flow. J. Biomech. Eng. 2010; 132(9):091005. [PubMed: 20815639]

86. Munn, LL.; Kamoun, W.; Dupin, M.; Tyrell, JA. Modeling structural and functional adaptation of tumor vessel networks during antiangiogenic therapy. In: Jackson, TL., editor. Modeling Tumor Vasculature: Molecular, Cellular, and Tissue Level Aspects and Implications. New York: Springer; 2012. p. 213-233.

87. Murphy EA, Majeti BK, Barnes LA, Makale M, Weis SM, Lutu-Fuga K, Wrasidlo W, Cheresh DA. Nanoparticle-mediated drug delivery to tumor vasculature suppresses metastasis. Proc. Natl Acad. Sci. USA. 2008; 105(27):9343–9348. [PubMed: 18607000]

88. Ng L, Bernard A, Lau C, Overly CC, Dong HW, Kuan C, Pathak S, Sunkin SM, Dang C, Bohland JW, Bokil H, Mitra PP, Puelles L, Hohmann J, Anderson DJ, Lein ES, Jones AR, Hawrylycz M. An anatomic gene expression atlas of the adult mouse brain. Nat. Neurosci. 2009; 12(3):356–362. [PubMed: 19219037]

89. Pathak AP. Magnetic resonance susceptibility based perfusion imaging of tumors using iron oxide nanoparticles. Wiley Interdisc. Rev. Nanomed. Nanobiotechnol. 2009; 1(1):84–97. [PubMed: 20049781]

90. Pathak AP, Hochfeld WE, Goodman SL, Pepper MS. Circulating and imaging markers for angiogenesis. Angiogenesis. 2008; 11(4):321–335. [PubMed: 18925424]

91. Pathak AP, Kim E, Zhang J, Jones MV. Threedimensional imaging of the mouse neurovasculature with magnetic resonance microscopy. PLoS ONE. 2011; 6(7):e22643. [PubMed: 21818357]

92. Pathak AP, Penet MF, Bhujwalla ZM. MR molecular imaging of tumor vasculature and vascular targets. Adv. Genet. 2010; 69:1–30. [PubMed: 20807600]

93. Pathak AP, Ward BD, Schmainda KM. A novel technique for modeling susceptibility-based contrast mechanisms for arbitrary microvascular geometries: the finite perturber method. Neuroimage. 2008; 40(3):1130–1143. [PubMed: 18308587]

94. Peng H. Bioimage informatics: a new area of engineering biology. Bioinformatics. 2008; 24(17):1827–1836. [PubMed: 18603566]

95. Perfahl H, Byrne HM, Chen T, Estrella V, Alarcon T, Lapin A, Gatenby RA, Gillies RJ, Lloyd MC, Maini PK, Reuss M, Owen MR. Multiscale modelling of vascular tumour growth in 3D: the roles of domain size and boundary conditions. PLoS ONE. 2011; 6(4):e14790. [PubMed: 21533234]

96. Popel AS, Johnson PC. Microcirculation and hemorheology. Annu. Rev. Fluid Mech. 2005; 37:43–69. [PubMed: 21151769]

97. Pries AR, Cornelissen AJ, Sloot AA, Hinkeldey M, Dreher MR, Hopfner M, Dewhirst MW, Secomb TW. Structural adaptation and heterogeneity of normal and tumor microvascular networks. PLoS Comput. Biol. 2009; 5(5):e1000394. [PubMed: 19478883]

98. Pries AR, Hopfner M, le Noble F, Dewhirst MW, Secomb TW. The shunt problem: control of functional shunting in normal and tumour vasculature. Nat. Rev. Cancer. 2010; 10(8):587–593. [PubMed: 20631803]

99. Pries AR, Reglin B, Secomb TW. Remodeling of blood vessels: responses of diameter and wall thickness to hemodynamic and metabolic stimuli. Hypertension. 2005; 46(4):725–731. [PubMed: 16172421]

100. Pries AR, Secomb TW. Microvascular blood viscosity in vivo and the endothelial surface layer. Am. J. Physiol. Heart Circ. Physiol. 2005; 289(6):H2657–H2664. [PubMed: 16040719]

101. Pries AR, Secomb TW, Gaehtgens P, Gross JF. Blood flow in microvascular networks. Experiments and simulation. Circ. Res. 1990; 67(4):826–834. [PubMed: 2208609]

102. Pries AR, Secomb TW, Gessner T, Sperandio MB, Gross JF, Gaehtgens P. Resistance to blood flow in microvessels in vivo. Circ. Res. 1994; 75(5):904–915. [PubMed: 7923637]

103. Qutub AA, Mac Gabhann F, Karagiannis ED, Vempati P, Popel AS. Multiscale models of angiogenesis. IEEE Eng. Med. Biol. Mag. 2009; 28(2):14–31. [PubMed: 19349248]

104. Rege A, Thakor NV, Rhie K, Pathak AP. In vivo laser speckle imaging reveals microvascular remodeling and hemodynamic changes during wound healing angiogenesis. Angiogenesis. 2012; 15(1):87–98. [PubMed: 22198198]

105. Reichold J, Stampanoni M, Lena Keller A, Buck A, Jenny P, Weber B. Vascular graph model to simulate the cerebral blood flow in realistic vascular networks. J. Cereb. Blood Flow Metab. 2009; 29(8):1429–1443. [PubMed: 19436317]

106. Rejniak KA, Anderson AR. Hybrid models of tumor growth. Wiley Interdiscip. Rev. Syst. Biol. Med. 2010; 3(1):115–125. [PubMed: 21064037]

107. Risser L, Plouraboue F, Steyer A, Cloetens P, Le Duc G, Fonta C. From homogeneous to fractal normal and tumorous microvascular networks in the brain. J. Cereb. Blood Flow Metab. 2007; 27(2):293–303. [PubMed: 16736048]

108. Ruoslahti E. Specialization of tumour vasculature. Nat. Rev. Cancer. 2002; 2(2):83–90. [PubMed: 12635171]

109. Schneider BP, Miller KD. Angiogenesis of breast cancer. J. Clin. Oncol. 2005; 23(8):1782–1790. [PubMed: 15755986]

110. Secomb TW, Dewhirst MW, Pries AR. Structural adaptation of normal and tumour vascular networks. Basic Clin. Pharmacol. Toxicol. 2011; 110(1):63–69. [PubMed: 21995550]

111. Secomb TW, Hsu R, Dewhirst MW, Klitzman B, Gross JF. Analysis of oxygen transport to tumor tissue by microvascular networks. Int. J. Radiat. Oncol. Biol. Phys. 1993; 25(3):481–489. [PubMed: 8436527]

112. Song JW, Munn LL. Fluid forces control endothelial sprouting. Proc. Natl Acad. Sci. USA. 2011; 108(37):15342–15347. [PubMed: 21876168]

113. Spilker RL, Feinstein JA, Parker DW, Reddy VM, Taylor CA. Morphometry-based impedance boundary conditions for patient-specific modeling of blood flow in pulmonary arteries. Ann. Biomed. Eng. 2007; 35(4):546–559. [PubMed: 17294117]

114. Stefanini MO, Qutub AA, Mac Gabhann F, Popel AS. Computational models of VEGF-associated angiogenic processes in cancer . Math. Med. Biol. 2011

115. Su SW, Catherall M, Payne S. The influence of network structure on the transport of blood in the human cerebral microvasculature. Microcirculation. 2011

116. Tang BT, Fonte TA, Chan FP, Tsao PS, Feinstein JA, Taylor CA. Three-dimensional hemodynamics in the human pulmonary arteries under resting and exercise conditions. Ann. Biomed. Eng. 2011; 39(1):347–358. [PubMed: 20640512]

117. Tozer GM, Ameer-Beg SM, Baker J, Barber PR, Hill SA, Hodgkiss RJ, Locke R, Prise VE, Wilson I, Vojnovic B. Intravital imaging of tumour vascular networks using multi-photon fluorescence microscopy. Adv. Drug Deliv. Rev. 2005; 57(1):135–152. [PubMed: 15518926]

118. Tsoukias NM, Goldman D, Vadapalli A, Pittman RN, Popel AS. A computational model of oxygen delivery by hemoglobin-based oxygen carriers in three-dimensional microvascular networks. J. Theor. Biol. 2007; 248(4):657–674. [PubMed: 17686494]

119. Vakoc BJ, Lanning RM, Tyrrell JA, Padera TP, Bartlett LA, Stylianopoulos T, Munn LL, Tearney GJ, Fukumura D, Jain RK, Bouma BE. Three-dimensional microscopy of the tumor microenvironment in vivo using optical frequency domain imaging. Nat. Med. 2009; 15(10): 1219–1223. [PubMed: 19749772]

120. van Vliet M, van Dijke CF, Wielopolski PA, ten Hagen TL, Veenland JF, Preda A, Loeve AJ, Eggermont AM, Krestin GP. MR angiography of tumor-related vasculature: from the clinic to the microenvironment. Radiographics. 2005; 25(Suppl 1):S85–S97. [PubMed: 16227499]

121. Verli FD, Rossi-Schneider TR, Schneider FL, Yurgel LS, de Souza MA. Vascular corrosion casting technique steps. Scanning. 2007; 29(3):128–132. [PubMed: 17477397]

122. Vermeulen PB, van Golen KL, Dirix LY. Angiogenesis, lymphangiogenesis, growth pattern, and tumor emboli in inflammatory breast cancer: a review of the current knowledge. Cancer. 2010; 116(11 Suppl):2748–2754. [PubMed: 20503405]

123. Vignon-Clementel IE, Figueroa CA, Jansen KE, Taylor CA. Outflow boundary conditions for 3D simulations of non-periodic blood flow and pressure fields in deformable arteries. Comput. Methods Biomech. Biomed. Eng. 2010; 13(5):625–640.

124. Walter T, Shattuck DW, Baldock R, Bastin ME, Carpenter AE, Duce S, Ellenberg J, Fraser A, Hamilton N, Pieper S, Ragan MA, Schneider JE, Tomancak P, Heriche JK. Visualization of image data fromcells to organisms. Nat.Methods. 2010; 7(3 Suppl):S26–S41. [PubMed: 20195255]

125. Wu J, Long Q, Xu S, Padhani AR. Study of tumor blood perfusion and its variation due to vascular normalization by anti-angiogenic therapy based on 3D angiogenic microvasculature. J. Biomech. 2009; 42(6):712–721. [PubMed: 19268290]

126. Yang J, Yu LX, Rennie MY, Sled JG, Henkelman RM. Comparative structural and hemodynamic analysis of vascular trees. Am. J. Physiol. Heart Circ. Physiol. 2010; 298(4):H1249–H1259. [PubMed: 20081111]

127. Yun S, Tearney G, de Boer J, Iftimia N, Bouma B. High-speed optical frequency-domain imaging. Opt. Express. 2003; 11(22):2953–2963. [PubMed: 19471415]

128. Zagorchev L, Oses P, Zhuang ZW, Moodie K, Mulligan-Kehoe MJ, Simons M, Couffinhal T. Micro computed tomography for vascular exploration. J. Angiogenes. Res. 2010; 2(7)

129. Zhou M, Sahni O, Kim HJ, Figueroa CA, Taylor CA, Shephard MS, Jansen KE. Cardiovascular flow simulation at extreme scale. Comput.Mech. 2010; 46(1):71–82.
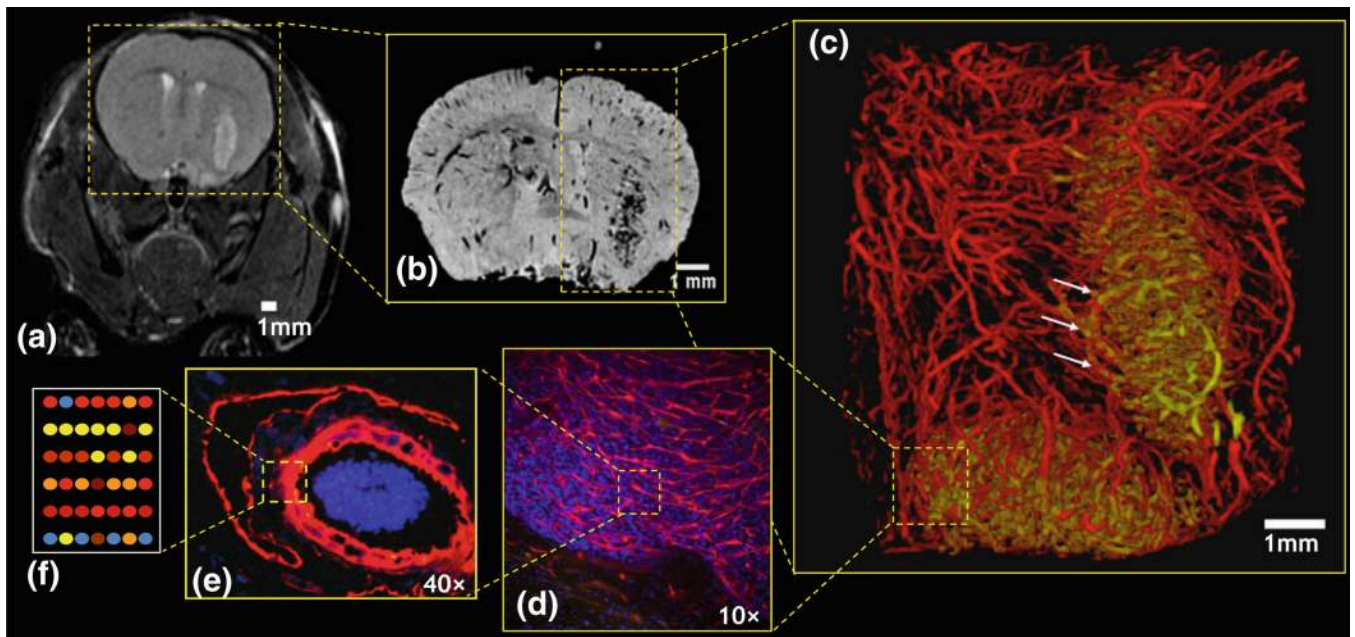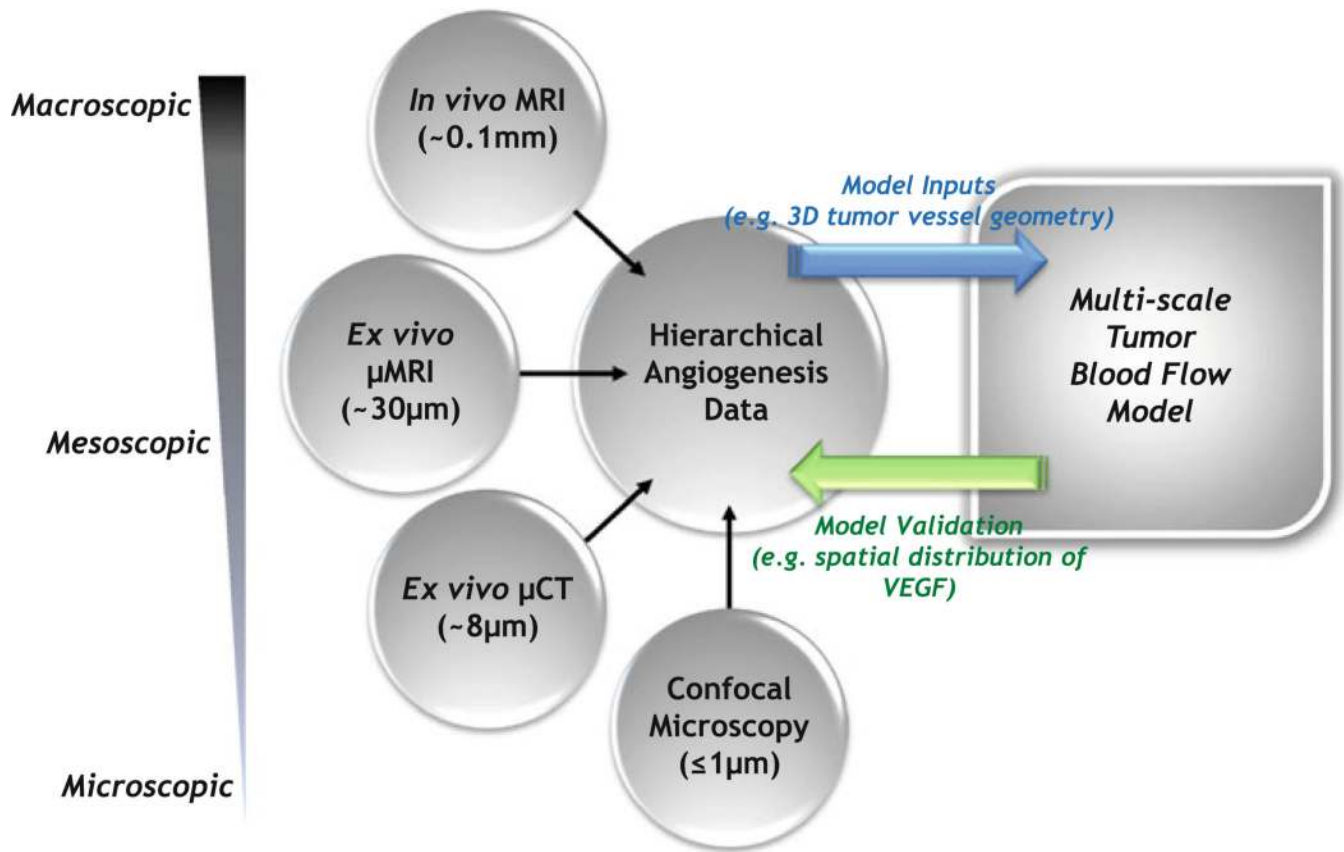
FIGURE 1.
Schematic illustrating "multiscale"imaging of the angiogenic phenotype. (a) *In vivo* MRI of a 9L brain tumor bearing mouse brain at the 'macroscopic' scale (~150 μm resolution); 3-D *ex vivo* MR microscopy (μMRI) at two 'mesoscopic' scales. (b) ~60 μm, and (c) ~30 μm in which the neurovasculature has been segmented into tumor vessels (gold) and cortical vessels (red). One can visualize the abnormal tumor vessel architecture and appreciate changes in vessel morphology at the tumor-host tissue interface (arrows). Imaging at the 'microscopic' scale: fluorescence microscopy images of (d) CD34 stained tumor vessels (10×), and (e) a lectin-labeled arteriole (40×). (f) Cartoon illustrating microarray analysis of the endothelium at the 'molecular' scale.
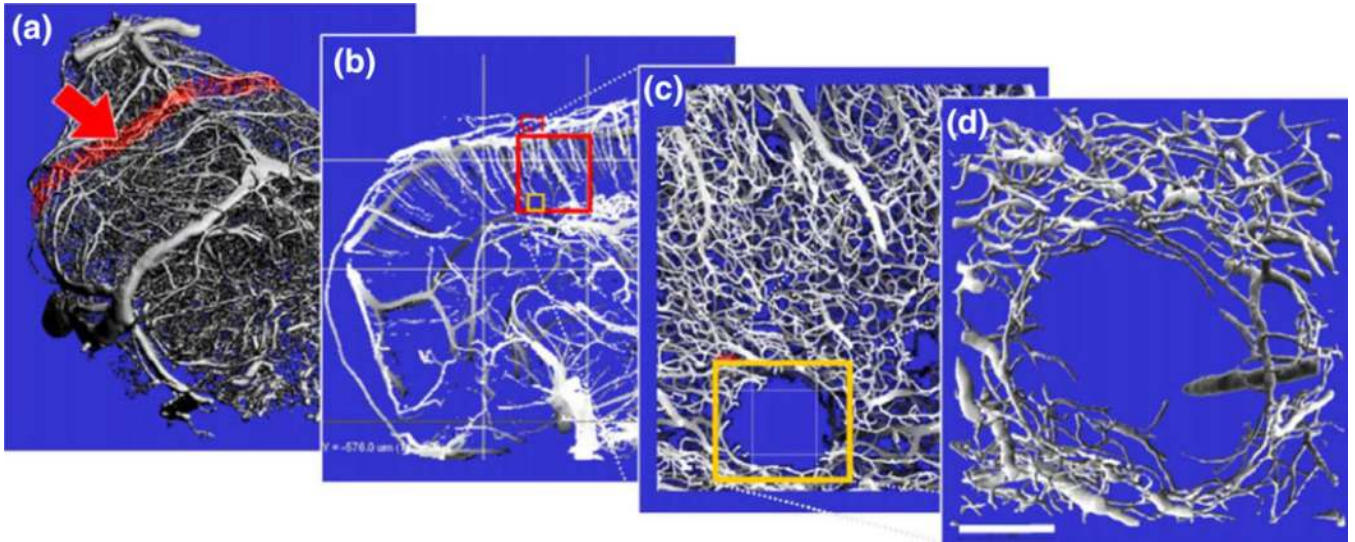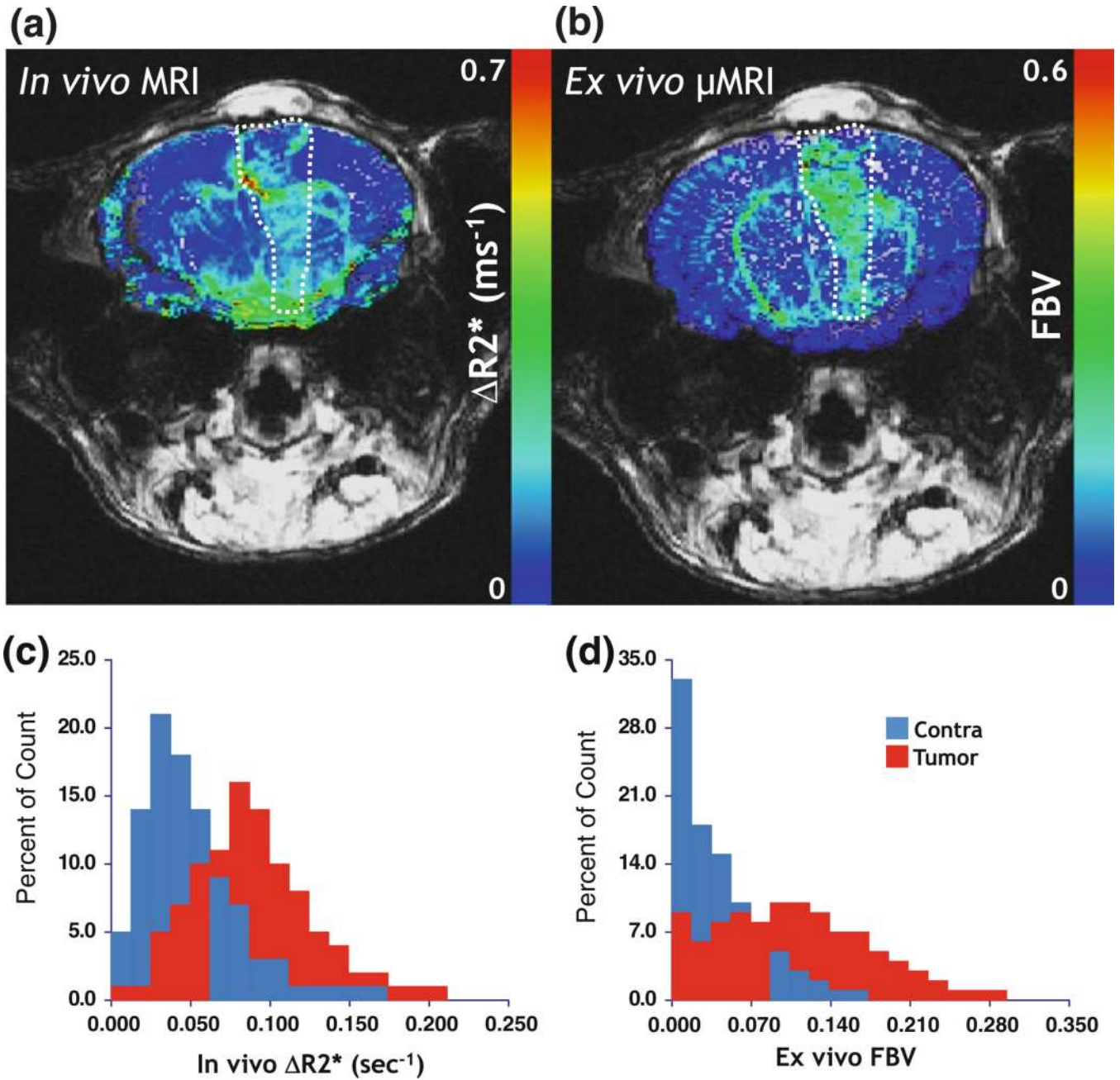
FIGURE 2.
Hierarchical imaging of the mouse brain vasculature. (a) Intact mouse brain vasculature scanned at medium resolution (16 μm voxel size) using a μCT system. (b) Slice of the section marked red in panel (a), revealing the frontal cortex. The red square labeled "C1"denotes a region of interest (ROI) which was measured using SRμCT. (c) Slice of SRμCT high-resolution data visualizing intracerebral arteries and the capillary network. The latter is not visualized in the medium resolution data (b) but provides essential structural characteristics of the vasculature, as for example the microinfarct marked by the red rectangle. (d) Surface rendering of the infarct region marked in panel (c) suitable for detailed 3-D analysis. Scale bar: 100 μm. (Adapted with kind permission from Heinzer *et al.*[47]).
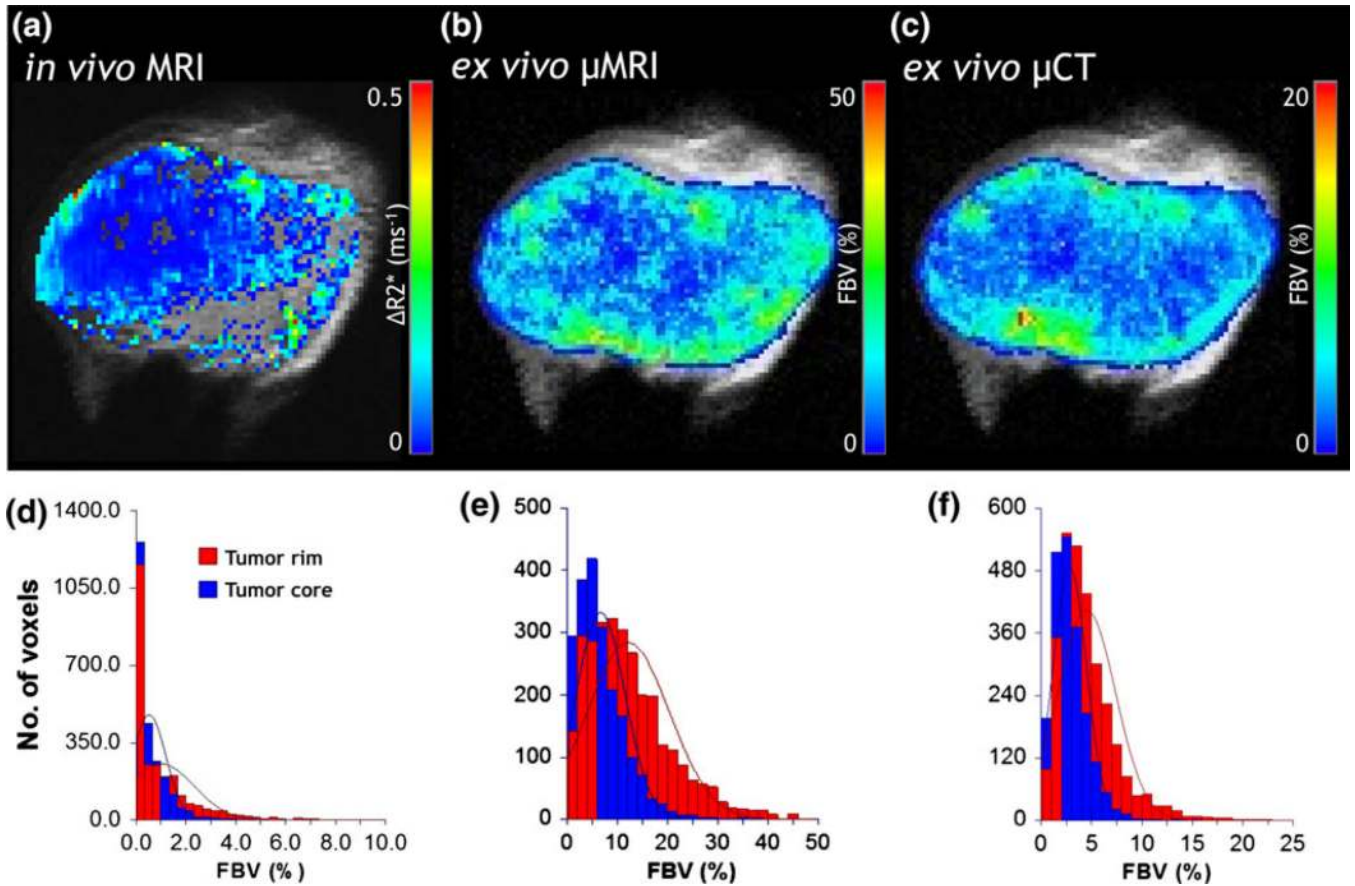
FIGURE 3.
Schematic illustrating the bidirectional feedback between multiscale imaging and multiscale modeling of tumor blood flow. Following acquisition of the hierarchical angiogenesis data, certain imaging parameters will serve as inputs to the multiscale model of tumor blood flow, while others will be employed to validate model predictions. For example, the μCT-derived 3-D tumor vessel geometry could serve as the input for large-scale tumor blood flow simulations. Predictions of the blood flow simulations will inform an oxygen transport model, which in turn will determine results of a VEGF secretion model. The VEGF secretion model will predict the spatio-temporal distribution of VEGF within the tumor, which will be validated against the spatial distribution of VEGF obtained from confocal microscopy of immunostained tumor sections. It should be borne in mind that acquiring macroscopic 2D (1 mm thick slices) *in vivo* MRI data over a 1–2 cm axial FOV at 125 μm in-plane resolution takes 5–10 min and results in ~MB of data. In contrast, a mesoscopic μMRI acquisition of the same volume at ~40–50 μm isotropic resolution takes 8–10 h, resulting in ~100 MB of data, while a microscopic μCT acquisition of the same volume at ~8 μm isotropic resolution takes 10–12 h, resulting in ~1 GB of data.
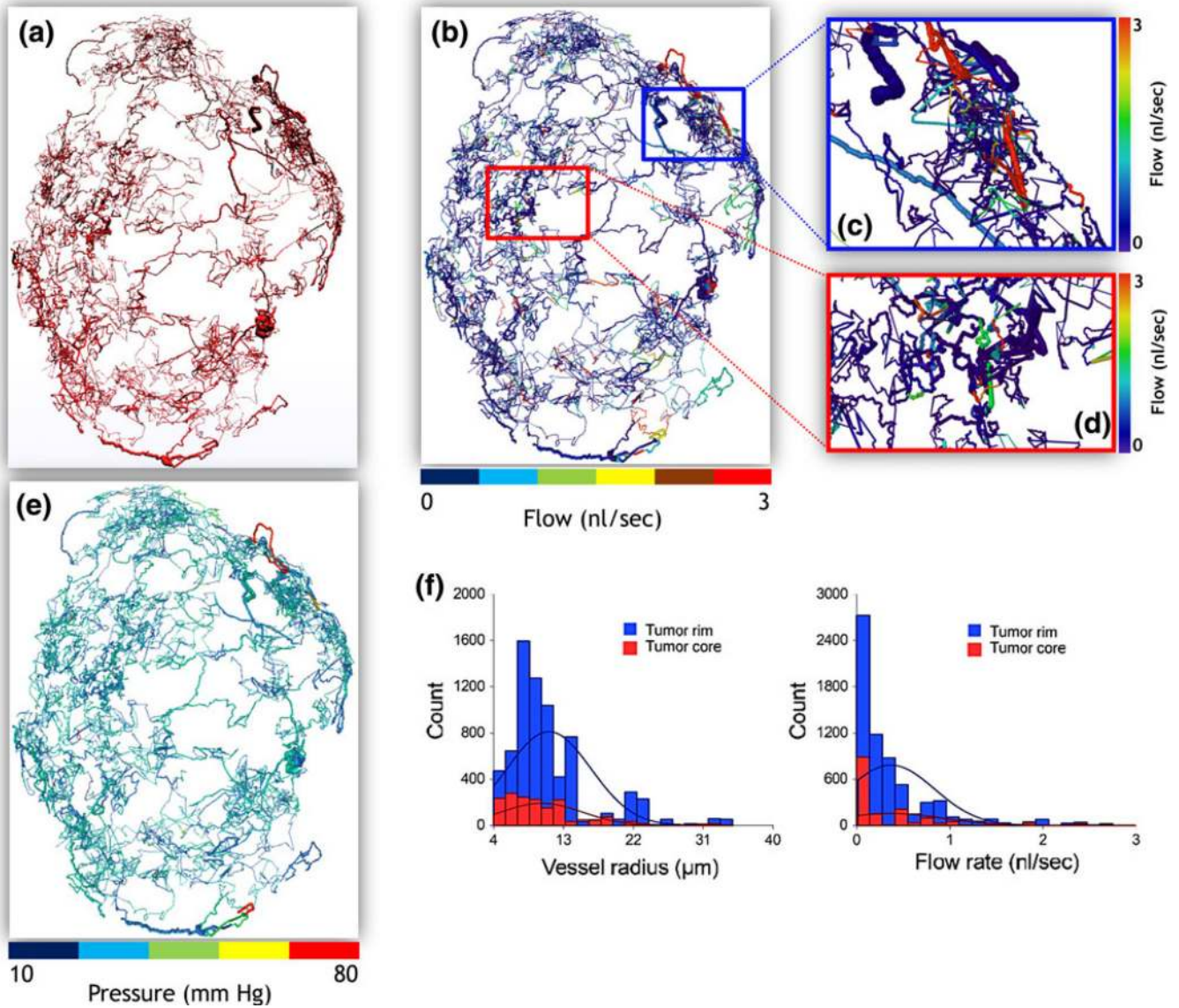
FIGURE 4.
Bridging "macroscale" and "microscale" with MRI. (a) *In vivo* macrovascular cerebral blood volume (CBV or ΔR_2^*) map. (b) Co-registered *ex vivo* fractional blood volume (FBV) map obtained from μMRI. The tumor region of interest (ROI) is highlighted by hatched lines in each panel. (c) Histograms showing the relative distribution of the ΔR_2^* between tumor and contralateral ROIs. (d) Histograms showing the relative distribution of the FBV between tumor and contralateral ROIs. Tumor blood volume is elevated relative to the contralateral brain across these "multi-scale" data. Adapted from Pathak *et al.*[91]

FIGURE 5.
Co-registered, multiscale blood volume maps in a human (MDA-MB-231) breast cancer model. (a) Macrovascular blood volume map computed from *in vivo* MRI (~100 μm). Co-registered maps of fractional blood volume (FBV) computed from (b) μMRI (~40 μm) and (c) μCT (~8 μm). One can differentiate the well-vascularized rim from the poorly vascularized tumor core in (a–c). (d–f) Distributions of FBV from each spatial scale demonstrating elevated blood volumes in the rim vs. the core for this xenograft model. The rim and core were identified using morphological erosion on a tumor 'mask' such that the numbers of pixels in the two regions were approximately equal. The lines superimposed on the histograms represent normal distributions fitted to the histogram data.

FIGURE 6.
Image-based hemodynamic modeling in a human breast cancer model. (a) Reconstructed "wide-area" 3-D microvascular network derived from μCT data acquired from a 5-week-old MDA-MB-231 breast cancer xenograft. (b) Blood flow map (in nl/s). Magnified blood flow maps corresponding to (c) a rim ROI (blue box), and (d) a more central ROI (red box). (e) Pressure distribution (in mmHg) for the entire tumor vasculature. (f) Radius (in μm) and blood flow (in nl/s) distributions corresponding to the tumor rim and core ROIs in (c–d). The lines superimposed on the histograms represent normal distributions fitted to the histogram data.

TABLE 1

Summary of representative macroscale image-based blood flow models.

System/organ	Mathematical formulation	Method	No. of cells	Imaging Method	Outlet boundary Conditions	Species	References
Intracranial aneurysm/brain	1-D Navier–Stokes/porous medium	Finite volume	10^7	DSA	WSS-scaled	Human	Augsburger et al.[4]
Intracranial aneurysm/brain	3-D Navier–Stokes	Finite volume	3×10^6	MRI	WSS-scaled	Human	Marzo et al.[81]
Intracranial arterial network	3-D/1-D Navier–Stokes	Spectral element	2×10^5	MRI	WK3/RC	Human	Grinberg et al.[44]
Systemic arterial tree	3-D Navier–Stokes	Finite element	10^9	CT	WK3	Human	Zhou et al.[129]
Carotid artery	3-D Navier–Stokes	Finite volume	9×10^5	CT	WK3/RC	Human	Morbiducci et al.[85]
Coronary arterial tree	3-D Navier–Stokes	Finite element	3×10^5	CT	Scaling Law	Pig	Huo et al.[53]
Pulmonary arterial tree	3-D Navier–Stokes	Finite element	1.5×10^6	MRI	Area-scaled	Human	Tang et al.[116]
Pulmonary arterial tree	1-D Navier–Stokes	Finite element	16×10^6	MRI	Morphometry-based	Human/Pig	Spilker et al.[113]

DSA: Digital Subtraction Angiography, MRI: Magnetic Resonance Imaging, CT: Computed Tomography.

TABLE 2

Summary of representative microvascular image-based blood flow simulations using the empirical hemorheological Pries–Secomb relationships.

System/organ	Imaging method	Outlet boundary conditions	Species	References
Intra-cortical vascular network	Confocal microscopy	Pressure/zero flow/flow rate	Human	Lorthois et al.[75]
Retinal microvasculature	Confocal microscopy	Pressure	Mouse	Ganesan et al.[42]
Retinal arterial microvasculature	Fundus camera	Structured tree	Human	Liu et al.[72]
Skeletal muscle microvasculature	Confocal microscopy	Pressure	Rat	Benedict et al.[9]
Coronary microvasculature	μCT	Pressure	Rat	Lee and Smith[69]
Intra-cortical vascular network	SRμCT	Pressure	Rat	Reichold et al.[105]
Fetoplacental and pulmonary vascular network	μCT	Pressure	Mouse	Yang et al.[126]

SRμCT: Synchrotron Radiation Based Micro-CT.